International Journal of Microwave and Wireless Technologies

cambridge.org/mrf

Low-profile closely coupled dual-band MIMO antenna using double layer metasurface

Dayu Qiao, Liping Han, Yufeng Liu, Wenmei Zhang and Member, IEEE

College of Physics and Electronic Engineering, Shanxi University, Taiyuan, China

Research Paper

Cite this article: Qiao D, Han L, Liu Y, Zhang W, Member, IEEE (2023). Low-profile closely coupled dual-band MIMO antenna using double layer metasurface. *International Journal of Microwave and Wireless Technologies* **15**, 1537–1544. https://doi.org/10.1017/S175907872300003X

Received: 4 August 2022
Revised: 11 January 2023
Accepted: 14 January 2023

Keywords:
Closely coupled; dual-band; low-profile; MIMO; MTS decoupling

Author for correspondence:
Liping Han,
E-mail: hlp@sxu.edu.cn

Abstract

A two-element low-profile closely coupled dual-band MIMO antenna is demonstrated for WiMAX applications. Based on the principle of metasurface (MTS) decoupling, a double-layer MTS consisting of pairs of elliptic patches with two different sizes is proposed. The MTS is loaded above a coupled dual-band MIMO antenna, and the mutual coupling in the lower and upper band is reduced by the larger and smaller elliptic patches, respectively. The edge-to-edge distance of antenna elements is only $0.01\lambda_0$ (λ_0 is the free-space wavelength at 2.6 GHz). The measured results show that the working bandwidths of the MIMO antenna are 2.5–2.69 and 3.4–3.69 GHz. The −10 dB impedance bandwidths in two bands are 8.83% (2.49–2.72 GHz) and 8.50% (3.38–3.68 GHz), and the isolation between antenna elements is enhanced by 13.5 and 18.4 dB in two bands, respectively. Moreover, broadside radiation performances in two bands are obtained.

Introduction

With the rapid development of mobile communication technology, multi-band antenna system becomes the main development trend due to its high data rate and channel capacity. Multiple-input-multiple-output (MIMO), as a key technique to improve channel capacity, has been widely used in wireless communication systems. The mutual coupling between the MIMO antenna elements degrades the system performance. Traditionally, there has been many methods for reducing the mutual coupling between multi-band MIMO antenna elements, such as decoupling network [1, 2], defective ground structure (DGS) [3] and electromagnetic band-gap (EBG) [4, 5]. In [2], a decoupling network composed of a pair of open-loop square ring resonators is introduced for the decoupling of dual-band antennas. In [3], a DGS composed of a slot with two meander lines inside is proposed to improve isolation of a MIMO antenna. In [5], a double-ring mushroom-like EBG is employed to achieve dual-band decoupling. However, the antennas in [1–5] still suffer the disadvantage of complex structure, low radiation efficiency and large edge-to-edge distance.

With the continuing pursuit of the miniaturization of a system platform, the antenna elements are closer to each other. However, the closely coupling between the elements leads to the reduction of the channel capacity and efficiency. In recent years, MTS has been widely used in closely coupled antenna decoupling, due to its strong electromagnetic wave regulation characteristics. Several closely coupled single-band MIMO antennas based on MTS decoupling have been reported. Wang *et al.* propose a MTS consisting of split ring resonators to enhance the isolation of the antenna more than 20 dB [6, 7]. In [8], a MTS formed by periodic ring slots is employed to achieve single-band decoupling more than 40 dB. In [9, 10], a double-layer MTS composed of rectangular patches is loaded to improve the isolation of antenna elements by 15 dB. Recently, some closely coupled dual-band MIMO antennas based on MTS decoupling have been reported. In [11], an array-antenna decoupling surface (ADS) consisting of compact square patches is adopted to reduce mutual coupling between the dual-band array antenna by 10 and 20.4 dB. In [12], a modified ADS is proposed to enhance the isolation by 28.5 dB in the lower band and a H-shaped DGS is loaded to enhance the isolation by 19.4 dB in the upper band. In [13], a double layer MTS formed by rectangular strips with different lengths is employed to improve the isolation of the dual-band MIMO antenna by 20 and 11 dB in two bands. For the aforementioned antennas, the lowest profile of the closely coupled dual-band antennas is $0.27\lambda_0$, which still suffers the disadvantage of high profile. Therefore, it is a great challenge to achieve low profile characteristic for closely coupled dual-band MIMO antennas based on MTS decoupling.

In this paper, a low-profile closely coupled dual-band MIMO antenna is proposed using MTS decoupling. Based on the principle of MTS decoupling, a double-layer MTS composed of pairs of elliptic patches with two different sizes is proposed. The MTS is loaded above a coupled dual-band MIMO antenna, and the mutual coupling in the lower and upper band is reduced by the larger and smaller elliptic patches, respectively. The edge-to-edge distance of antenna elements is only $0.01\lambda_0$ and the profile height is $0.09\lambda_0$. The measurement results

© The Author(s), 2023. Published by Cambridge University Press in association with the European Microwave Association

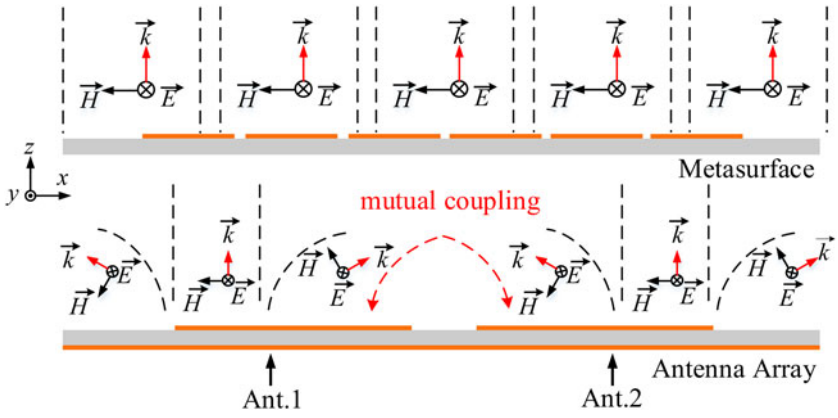

Fig. 1. Principle of MTS decoupling.

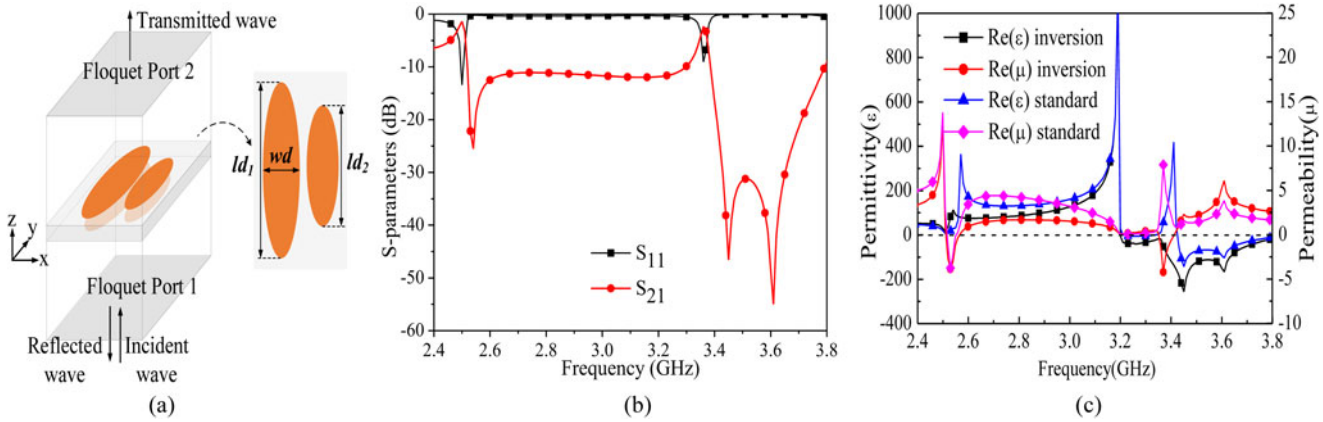

Fig. 2. MTS unit cell, (a) simulation model; (b) *S*-parameters; (c) permittivity and permeability.

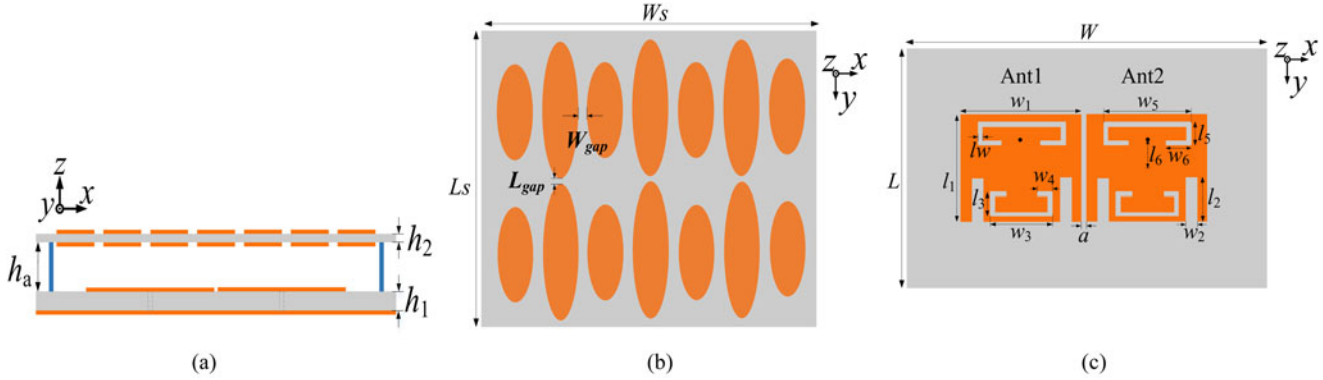

Fig. 3. Configuration of antenna structure, (a) side view; (b) top view of MTS; (c) top view of the coupled MIMO antenna.

show that the MIMO antenna can work in 2.5–2.69 and 3.4–3.69 GHz, and the isolation is enhanced by 13.5 and 18.4 dB in two bands, respectively. Moreover, broadside radiation performances in two bands are obtained.

Dual-band MIMO antenna based on MTS

Principle of MTS decoupling

A two-element MIMO antenna can be equivalent to a two-port network, and its relationship of input and output voltages is expressed by *S*-parameters [14]:

$$\begin{bmatrix} V_1^o \\ V_2^o \end{bmatrix} = \begin{bmatrix} S_{11} & S_{12} \\ S_{21} & S_{22} \end{bmatrix} \begin{bmatrix} V_1^i \\ V_2^i \end{bmatrix} \quad (1)$$

where S_{11} and S_{22} are the reflection coefficients of two ports, S_{12} and S_{21} are the coupling coefficients, V_1^i, V_2^i, V_1^o and V_2^o are the input and output voltages of two ports, respectively. When the network is lossless, reciprocal and matched, formula (1) can be

https://doi.org/10.1017/S175907872300003X Published online by Cambridge University Press

Table 1. Dimensions of antenna structure (Unit: mm)

L	W	l_1	w_1	l_2	w_2	l_3	w_3	l_w
70	100	34.5	35.5	13	3	5.5	24	1.5
w_4	l_5	w_5	l_6	w_6	a	L_s	W_s	l_{gap}
6.5	7	29	11.5	7.7	1	103	100	1.5
w_{gap}	h_a	h_1	h_2	l_{d1}	l_{d2}	w_d		
2.6	6	3	1	48.8	39	10.4		

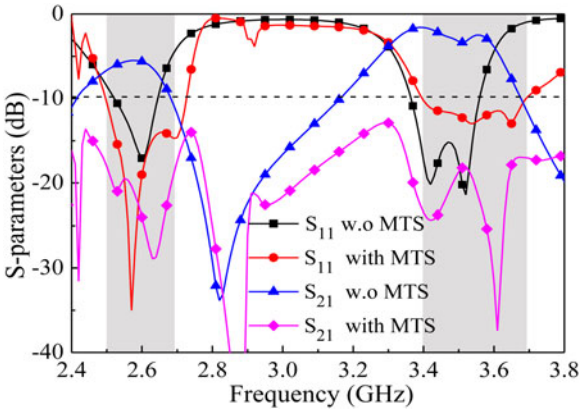

Fig. 4. *S*-parameters of antenna with/without MTS.

expressed as:

$$\begin{bmatrix} V_1^o \\ V_2^o \end{bmatrix} = \begin{bmatrix} 0 & S_{12} \\ S_{21} & 0 \end{bmatrix} \begin{bmatrix} V_1^i \\ V_2^i \end{bmatrix} \quad (2)$$

When $S_{12} = S_{21}$, the mutual coupling between two antenna elements will disappear, and the mutual impedances Z_{12} and Z_{21} should be reactive, thus the single negative metamaterial can be employed to reduce mutual coupling.

The principle of MTS decoupling is shown Fig. 1. A two-element MIMO antenna is arranged along the x-axis, and a single negative MTS is placed above the antenna, when the Ant.1 is excited and the Ant.2 is terminated with a 50 Ω matched load. The coupled electromagnetic waves propagate along the positive x-direction. When loading a single negative metamaterial ($\varepsilon_r < 0, \mu_r > 0$ or $\varepsilon_r > 0, \mu_r < 0$), the wavenumber k can be expressed as [6]:

$$k = w\sqrt{\mu \cdot \varepsilon} = \omega \cdot \sqrt{\varepsilon_r \varepsilon_0 \cdot \mu_r \mu_0} = jk_0 \cdot \sqrt{|\mu_r| \cdot |\varepsilon_r|} \quad (3)$$

The electric field along the positive x-direction can be expressed as:

$$E(x, t) = E_0 e^{jkx} e^{jwt} = E_0 e^{-k_0\sqrt{|\mu_r||\varepsilon_r|}\cdot x} \cdot e^{jwt} \quad (4)$$

Therefore, the coupled electric field along the x-axis is evanescent, and the electromagnetic wave mainly propagates along the z-direction. In a word, the mutual coupling between antenna elements can effectively reduce by loading the single negative MTS.

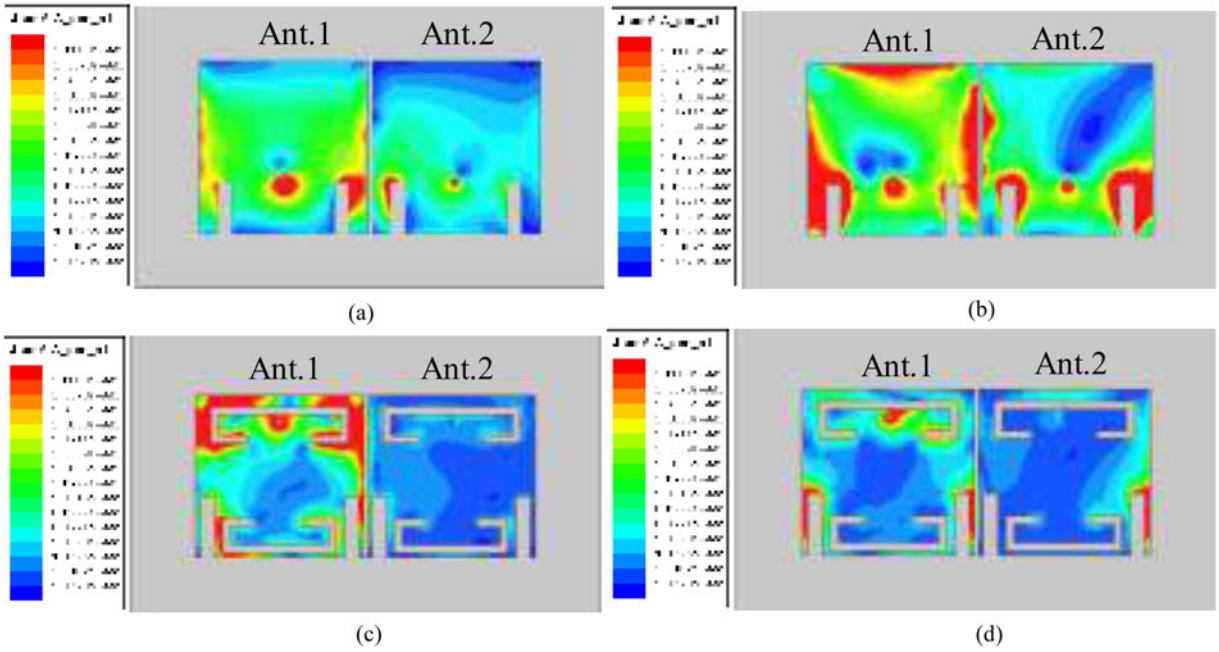

Fig. 5. Surface current distribution of antenna, (a) at 2.6 GHz without MTS; (b) at 3.5 GHz without MTS; (c) at 2.6 GHz with MTS; (d) at 3.5 GHz with MTS.

https://doi.org/10.1017/S175907872300003X Published online by Cambridge University Press

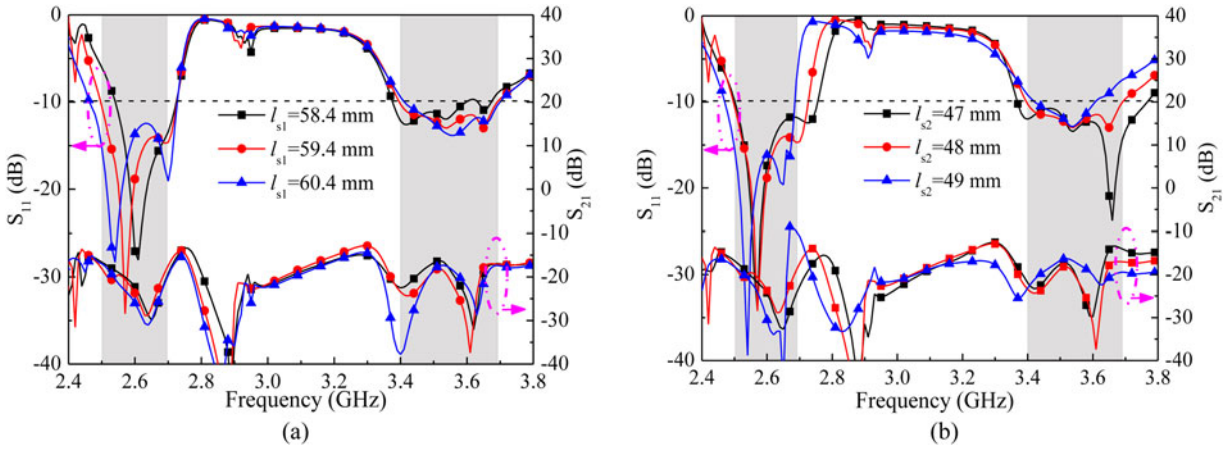

Fig. 6. *S*-parameters for different length of C-shaped slots, (a) l_{s1}; (b) l_{s2}.

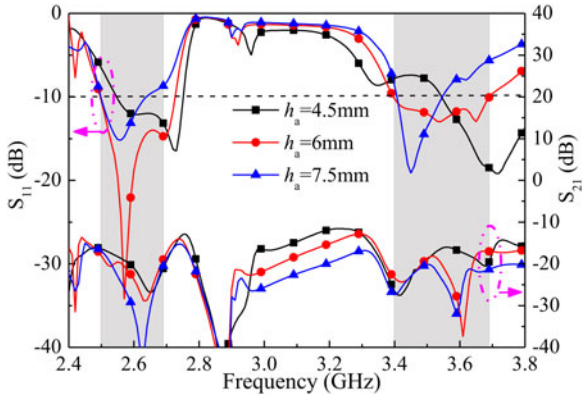

Fig. 7. *S*-parameters for different h_a.

MTS unit cell

Figure 2 plots the configuration of an unsymmetrical double-layer MTS unit cell. It consists of pairs of elliptic patches with two different sizes and is printed on the F4B substrate with a dielectric contains of 2.2, a loss tangent of 0.002 and a thickness of 1 mm. The master-slave boundaries are assigned on the sidewalls, and a pair of Floquet ports are applied on the *x*–*y* plane, as plotted in Fig. 2(a). The reflection and transmission coefficients of the unsymmetrical double-layer MTS unit cell are simulated with ANSYS HFSS. As shown in Fig. 2(b), the reflective type MTS unit cell operates at 2.6 and 3.5 GHz, and the electromagnetic waves can radiate effectively due to the anisotropic nature of the MTS [10]. The permittivity ε and permeability μ of the MTS unit cell are extracted using the standard parameter retrieval method [15] and the inversion algorithm [16] programmed by MATLAB in Appendix. Figure 2(c) plots the extracted ε and μ of the unit cell illuminated by *y*-polarized plane wave, it is observed that the results of two algorithms agree well. The ε and μ are positive and negative around 2.6 GHz while negative and positive around 3.5 GHz. Besides, the extracted permittivity has a spike at 3.2 GHz due to the coupling between the elliptic patches with different sizes in different layers.

Closely coupled dual-band MIMO antenna based on MTS

The configuration of the closely coupled dual-band MIMO antenna is shown in Fig. 3. A double-layer MTS formed by the proposed unit cells is loaded above a two-port coupled dual-band MIMO antenna to reduce the mutual coupling between the antenna elements. A pair of open slots is etched on the antenna element to achieve dual-band and two C-shape slots with different lengths are etched to increase the matching bandwidths in the lower and upper band, respectively. Two rows of the MTS unit cells are chosen to obtain better decoupling performance, and the distance between the MTS and the coupled antenna is determined by the theory of Fabry–Perot (F–P) cavity [17]. The coupled MIMO antenna is fabricated on the F4B substrate with a dielectric contains of 2.2 and a loss tangent of 0.002. The edge-to-edge distance of two antenna elements is 1 mm ($0.01\lambda_0$

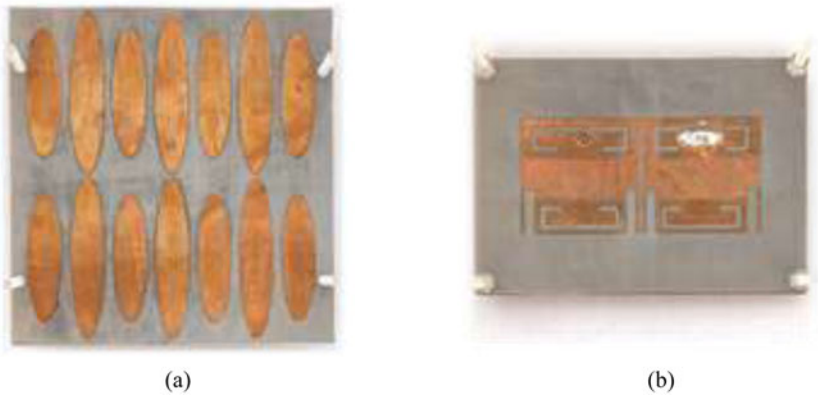

Fig. 8. Photograph of antenna, (a) MTS; (b) coupled MIMO antenna.

https://doi.org/10.1017/S175907872300003X Published online by Cambridge University Press

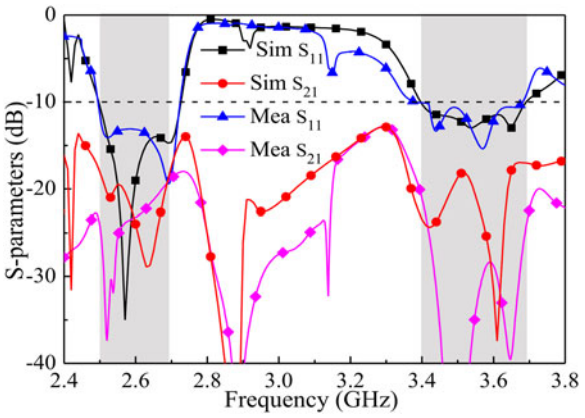

Fig. 9. *S*-parameters of antenna.

at 2.6 GHz). All analysis and simulations are carried out by HFSS 13.0, and the dimensions are listed in Table 1. Figure 4 shows the simulated *S*-parameters of the antenna with/without MTS. It can be seen that, the bandwidth in the lower band is increased from 4.26% (2.53–2.64 GHz) to 8.43% (2.5–2.72 GHz) and that in the upper band is increased from 4.62% (3.38–3.54 GHz) to 8.18% (3.4–3.69 GHz). Also, after loading the MTS, the isolation in two bands is improved by 12.5 and 15.4 dB, respectively.

A thinner substrate minimizes the surface waves and the mutual coupling between the closely coupled antennas is mainly due to the near-field space waves. The surface current distribution for antenna with/without MTS is investigated to illustrate the working mechanism of the MTS for mutual coupling reduction. Figure 5 shows the surface current distribution of the antenna when the Ant.1 is excited and the Ant.2 is terminated by a 50 Ω load. It is observed that without the MTS, a strong coupling current is distributed on the Ant. 2. However, after loading the MTS, the coupling current on the Ant. 2 at two bands is dramatically reduced as shown in Figs 5(c) and 5(d). In other words, the MTS has the favorable decoupling capability for a dual-band MIMO antenna.

Parametric analysis

The effect of the structural parameters on the antenna performance is conducted. It is found that the length of C-shape slots ($ls_1 = w_5 + 2 \times l_5 + 2 \times w_6$, $ls_2 = w_3 + 2 \times l_3 + 2 \times w_4$) and the

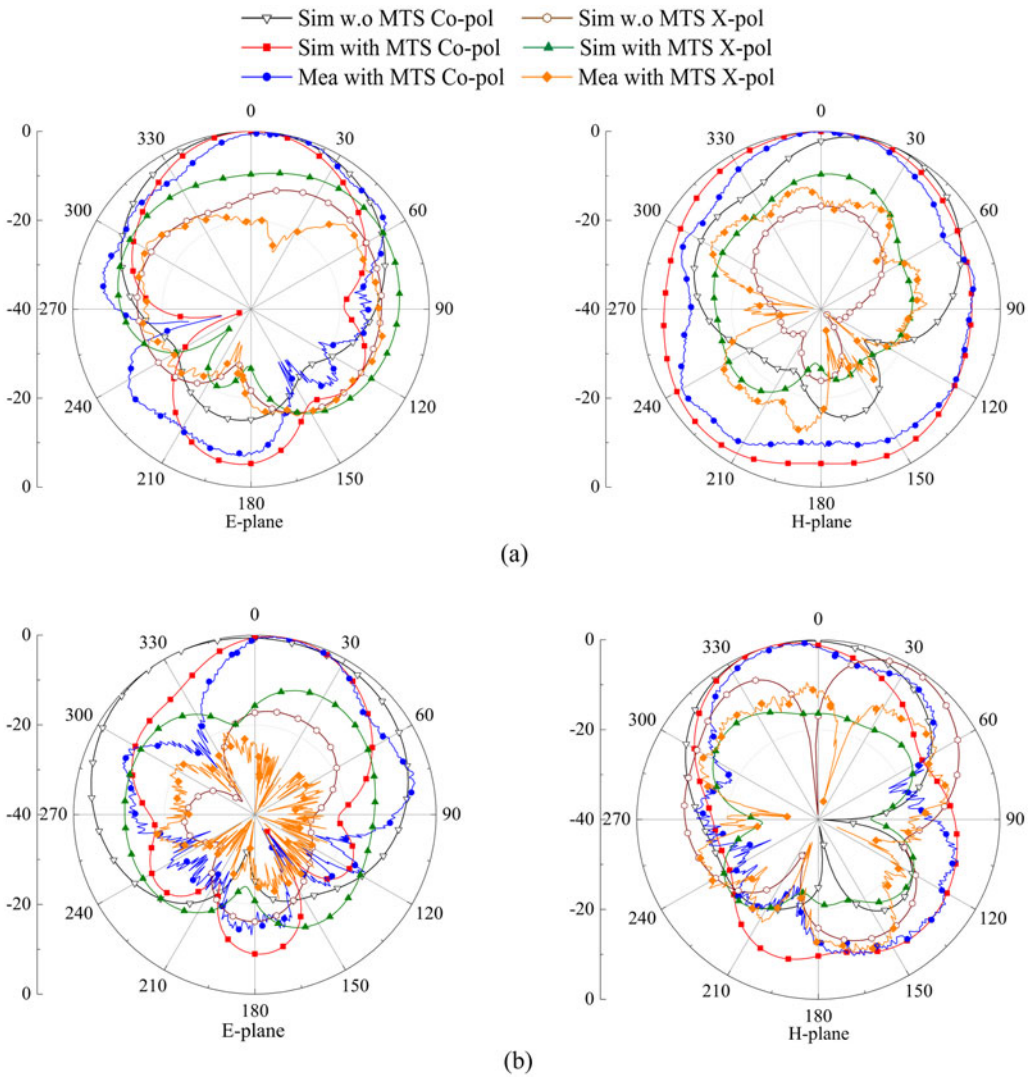

Fig. 10. Radiation patterns when the Ant.1 is excited, (a) at 2.6 GHz; (b) at 3.5 GHz.

https://doi.org/10.1017/S175907872300003X Published online by Cambridge University Press

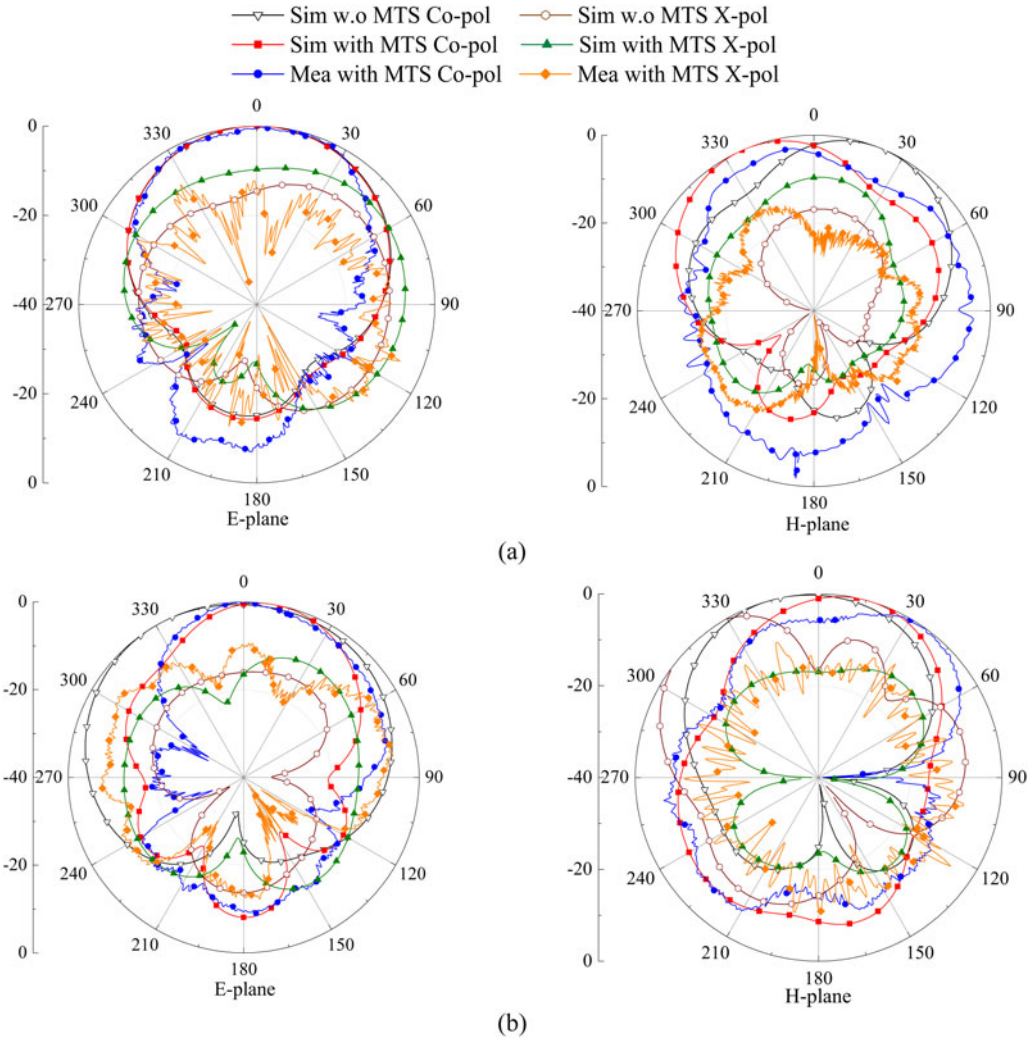

Fig. 11. Radiation patterns when the Ant.2 is excited, (a) at 2.6 GHz; (b) at 3.5 GHz.

distance between the MTS and coupled antenna (h_a) play a significant role.

Figure 6 shows the *S*-parameters for different ls_1 and ls_2. It is observed that the length of C-shape slots has significant effects on the impedance bandwidths and slight effects on the isolation.

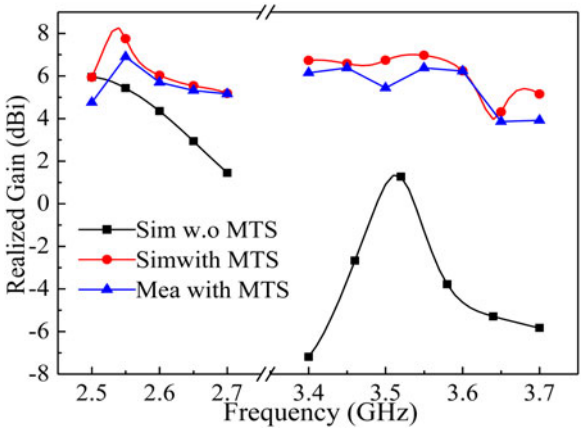

Fig. 12. Gain of antenna.

With the decrease of ls_1, the impedance bandwidth in the lower band decreases, while that in the upper band is insensitive to ls_1. When ls_2 decreases, the bandwidth in the lower band increases and that in the upper band increases significantly. As shown in Fig. 7, the resonance frequency and isolation are sensitive to h_a. With the decrease of h_a, the resonance in the lower band increases and the second resonance of the upper band increases significantly. In a word, the resonance frequency could be controlled by h_a. Meanwhile, the decoupling effect in two bands becomes poorer with the decrease of h_a. When ls_1 = 59.4 mm, ls_2 = 48 mm, h_a = 6 mm, the S_{11} of antenna covers 2.5–2.69 and 3.4–3.69 GHz, and the S_{21} is below −18 and −17 dB in two bands.

Experimental results

A prototype of the proposed closely couple dual-band MMO antenna is fabricated and measured. Figure 8 shows the photographs of the MIMO antenna. The *S*-parameter is measured by an Agilent N5221A vector network analyzer, and the radiation pattern is measured by a Lab-Volt 8092 antenna training and measuring system.

https://doi.org/10.1017/S175907872300003X Published online by Cambridge University Press

Table 2. Performance comparison of dual-band antennas based on MTS decoupling

Ref.	Center Fre. (GHz)	Bandwidth (%)	Edge-to-edge distance (λ_0)	Height (λ_0)	Promotion in isolation (dB)
[11]	4.5/5.6	1.1/1.6	0.18	0.34	10/20.4
[12]	3.7/4.1	1.48/2.07	0.03	0.33	28.5/19.4
[13]	2.6/3.5	7.69/5.71	0.01	0.21	20/11
Pro.	2.6/3.5	7.69/8.45	0.01	0.09	13.5/18.4

Figure 9 shows the measured and simulated *S*-parameters of the antenna. It is seen that the measured results agree basically with the simulated ones and the measured isolation is deeper than the simulated one. The simulated −10 dB impedance bandwidths of two bands are 8.43% (2.5–2.72 GHz) and 8.18% (3.4–3.69 GHz), and the corresponding isolation between antenna elements is improved to 18 and 17 dB in two bands. The measured results show that the −10 dB impedance bandwidths of two bands are 8.83% (2.49–2.72 GHz) and 8.50% (3.38–3.68 GHz), and the isolation can be improved to 19 and 20 dB, respectively. The difference between the measurement and simulation results is mainly due to the fabrication errors and the deviation of dielectric constant.

Figures 10 and 11 show the simulated and measured patterns when the Ant.1 and Ant.2 are independently excited. It can be seen that a good agreement between the simulated and measured results is obtained. After loading the MTS, the dual-band MIMO antenna remains stable broadside radiation patterns except the cross-polarization are slightly changed. Meanwhile, the significant back radiation and the wider beamwidth with MTS is mainly because the MTS substrate is larger than the coupled antenna substrate. Figure 12 shows the simulated and measured gains. It is known that the MTS could be regarded as a superstrate to improve the gain of antenna, and the flat gain is obtained by forming a Fabry–Perot cavity [18]. The peak gains of the MIMO antenna with MTS are improved to 8.26 and 7 dBi in two bands, and the measured ones are 6.9 and 6.38 dBi, respectively.

Finally, Table 2 lists the comparison of the reported and proposed closely couple dual-band antennas based on MTS. It is observed that the proposed antenna has the lowest profile. Compared to the antennas with smaller bandwidths [11, 12], the antenna in this work has the smallest edge-to-edge distance. Moreover, the proposed antenna has bigger bandwidth in the upper band compared to the antenna in [13].

Conclusion

This paper presents a low-profile closely coupled dual-band MIMO antenna for WiMAX applications. A double-layer MTS composed of pairs of elliptic patches is loaded above the dual-band coupled antenna to reduce the mutual coupling. The edge-to-edge distance between antenna elements is only 1 mm ($0.01\lambda_0$) and the profile height is 10 mm ($0.09\lambda_0$). The measured results show that the −10 dB impedance bandwidths of the dual-band MIMO antenna are 8.83 and 8.50%, and the isolation in two bands is improved by 13.5 and 18.4 dB, respectively. Also, the proposed antenna has potential to decouple dual-band antenna array with more elements.

Data. Data sharing is not applicable to this article as no new data were created or analyzed in this study.

Acknowledgements. Dayu Qiao is the first author, Professor Liping Han is the corresponding author. Thanks to Yufeng Liu and Professor Wenmei Zhang for their suggestions and guidance on this research.

Author contributions. Dayu Qiao performed the simulations, Professor Liping Han guided the design, Yufeng Liu and Professor Wenmei Zhang provided support during the experiment. All authors contributed equally to analyzing data and reaching conclusions, and in writing the paper.

Financial support. This work was supported by National Science Foundation of China (62071282) and National Science Foundation of Shanxi Province (201901D111026).

Conflict of interest. The authors report that they have no known conflict of interests or personal relationships that could have appeared to influence the work reported in this paper.

References

1. **Li M, Jiang L and Yeung KL** (2021) Design of dual-band decoupling network for two antennas. *IEEE International Symposium on Antennas and Propagation and USNC-URSI Radio Science Meeting (APS/URSI),* Singapore, Singapore.
2. **Zhao L and Wu K** (2015) A dual-band coupled resonator decoupling network for two coupled antennas. *IEEE Transactions on Antennas and Propagation* **63**, 2843–2850.
3. **Cheung SW, Li Q, Wu D, Zhou C and Wang B** (2017) Defected ground structure with two resonances for decoupling of dual-band MIMO antenna. *IEEE International Symposium on Antennas and Propagation & USNC/URSI National Radio Science Meeting,* San Diego, CA, USA.
4. **Tan X, Wang W, Wu Y, Liu Y and Kishk AA** (2019) Enhancing isolation in dual-band meander-line multiple antenna by employing split EBG structure. *IEEE Transactions on Antennas and Propagation* **64**, 2769–2774.
5. **Bai M, Ren W, Xue Z and Li W** (2019) The design of EBG for enhancing the isolation in dual-band microstrip antennas. *Photonics & Electromagnetics Research Symposium – Fall (PIERS – Fall),* Xiamen, China.
6. **Wang Z, Li C and Yin Y** (2020) A meta-surface antenna array decoupling (MAAD) design to improve the isolation performance in a MIMO system. *IEEE Access* **8**, 61797–61805.
7. **Wang Z, Li C, Wu Q and Yin Y** (2020) A metasurface-based low-profile array decoupling technology to enhance isolation in MIMO antenna systems. *IEEE Access* **8**, 125565–125575.
8. **Luan H, Chen C, Chen W, Zhou L, Zhang H and Zhang Z** (2019) Mutual coupling reduction of closely E/H-plane coupled antennas through metasurfaces. *IEEE Antennas and Wireless Propagation Letters* **18**, 1996–2000.
9. **Guo J, Liu F, Zhao L, Yin Y, Huang G-L and Li Y** (2019) Meta-surface antenna array decoupling designs for two linear polarized antennas coupled in H-plane and E-plane. *IEEE Access* **7**, 100442–100452.
10. **Liu F, Guo J, Zhao L, Shen X and Yin Y** (2019) A meta-surface decoupling method for two linear polarized antenna array in Sub-6 GHz base station applications. *IEEE Access* **7**, 2759–2768.
11. **Zou X-J, Wang G-M, Bai H, Hou H-S, Zong B-F and Wang Y-W** (2020) Array-antenna decoupling surface for dual-band microstrip antenna array. *International Conference on Microwave and Millimeter Wave Technology (ICMMT),* Shanghai, China.

https://doi.org/10.1017/S175907872300003X Published online by Cambridge University Press

12. **Niu Z, Zhang H, Chen Q and Zhong T** (2019) Isolation enhancement in closely coupled dual-band MIMO patch antennas. *IEEE Antennas and Wireless Propagation Letters* **18**, 1686–1690.
13. **Liu F, Guo J, Zhao L, Huang G-L, Li Y and Yin Y** (2020) Dual-band metasurface-based decoupling method for two closely packed dual-band antennas. *IEEE Transactions on Antennas and Propagation* **68**, 552–557.
14. **Bait-Suwailam MM, Boybay MS and Ramahi OM** (2010) Electromagnetic coupling reduction in high-profile monopole antennas using single-negative magnetic metamaterials for MIMO applications. *IEEE Transactions on Antennas and Propagation* **9**, 2894–2902.
15. **Szabó Z, Park G-H, Hedge R and Li E-P** (2010) A unique extraction of metamaterial parameters based on Kramers–Kronig relationship. *IEEE Transactions on Microwave Theory and Techniques* **58**, 2646–2653.
16. **Smith DR, Vier DC, Koschny T and Soukoulis CM** (2005) Electromagnetic parameter retrieval from inhomogeneous metamaterials. *Physical Review. E, Statistical, Nonlinear, and Soft Matter Physics* **71**, 036617.
17. **Cao W, Zhang H and Li S** (2016) Low-profile double-frequency Fabry-Perot (F-P) cavity antenna. *11th International Symposium on Antennas. Propagation and EM Theory (ISAPE),* Guilin, China.
18. **Singh AK, Abegaonkar MP and Koul SK** (2017) High-gain and high-aperture-efficiency cavity resonator antenna using metamaterial superstrate. *IEEE Antennas and Wireless Propagation Letters* **16**, 2388–2391.

Appendix

This appendix presents the inversion algorithm [16] programmed in MATLAB that was applied to compute the permittivity and permeability of the MTS design.

```
Freq = par_11(:,1);
s11_mag = par_11(:,2);
s11_ang = par_11(:,3)*pi/180;
s21_mag = par_21 (:,2);
s21_ang = par_21(:,3)*pi/180;
s11_real = s11_mag.*cos(s11_ang);
s11_im = s11_mag.*sin(s11_ang);
s21_real = s21_mag.*cos(s21_ang);
s21_im = s21_mag.*sin(s21_ang);
s11 = s11_real + i* s11_im;
s21 = s21_real + i*s21_im;
d = 0.0025;
k = 2*pi*Freq*10^9/(3*10^8);
alpha = (1 − s11.^2 + s21.^2)./(2*s21);
x = (1./(k*d)).*acos(alpha);
for g = 1:length(x)-1
x(g) = x(g)*sign(imag(alpha(g)));
end
n = (real(x)) + i*abs(imag(x));
y = −sqrt(((1 + s11).^2 − s21.^2)./((1 − s11).^2 − s21.^2));
z = abs(real(y)) + i*(imag(y));
ε = n./z;
μ = n.*z;
```

Dayu Qiao received the B.S. degree in electronic information engineering from Shanxi University, Taiyuan, China in 2020. Currently, she is pursuing the M.S. degree in information and communication engineering, Shanxi University, Taiyuan, China. Her research interests include decoupling of closely coupled MIMO antenna.

Liping Han received the B.S., M.S., and Ph.D. degrees in electronic engineering from Shanxi University, Taiyuan, China, in 1993, 2002, and 2010, respectively. Currently, she is a professor with the School of Physics and Electronic Engineering, Shanxi University. Her research interests include microwave and millimeter-wave integrated circuits and microstrip antenna.

Yufeng Liu was born in Shanxi Lvliang, China, in 1986. He received the Ph.D. degree in radio physics from Sichuan University, Sichuan, China, in 2014. In 2015, he joined the College of Physics and Electronic Engineering, Shanxi University. His research is mainly focused on computational electromagnetics and antenna design.

Wenmei Zhang received the B.S. and M.S. degrees in electronic engineering from Nanjing University of Science and Technology, Nanjing, China, in 1992 and 1995, respectively, and the Ph.D. degree in electronic engineering from Shanghai Jiao Tong University, Shanghai, China, in 2004. Currently, she is a professor with the School of Physics and Electronic Engineering, Shanxi University, Taiyuan, China. Her research interests include microwave and millimeter-wave integrated circuits, EMC, and microstrip antenna.

https://doi.org/10.1017/S175907872300003X Published online by Cambridge University Press